International Journal on Interactive Design and Manufacturing (IJIDeM)
https://doi.org/10.1007/s12008-023-01473-8

ORIGINAL PAPER

Predicting the thermal performance of screen mesh wick heat pipe with alumina nanofluids using response surface methodology

P. Lakshmi Reddy[1,2] · B. Sreenivasa Reddy[2] · K. Govindarajulu[3] · Din Bandhu[4] · Ashish Saxena[5]

Received: 6 June 2023 / Accepted: 31 July 2023
© The Author(s) 2023

Abstract
This study aims to investigate the effect of heat load, tilt angle, and volume concentration of alumina nanofluid on the thermal performance enhancement of cylindrical screen mesh wick heat pipe in terms of thermal resistance(R) and thermal conductivity(k). Response surface methodology based on the Box–Behnken design was implemented to investigate the influence of heat input (100–200 W), tilt angle (0–90°), and volume concentration (0.05–0.25 vol%) of nanofluid as the independent variables. Second-order polynomial equations were established to predict the responses, 'R', and 'k'. The significance of the models was tested by means of analysis of variance (ANOVA). In addition, a correlation between the independent variables was derived in this study. The results revealed that the optimum heat input, inclination angle, and concentration of nanofluid were determined as 200 W, 52.72°, and 0.1773 vol. % respectively for both 'R' and 'k'. SEM analysis was performed to observe the thermal performance phenomena of the heat pipe before and after experimentation.

Keywords Heat pipe · RSM · Thermal resistance · Thermal conductivity · Inclination angle · Nanofluid

1 Introduction

In electronic devices and electronic circuits, more failures take place due to the high operating temperatures. Due to this, thermal management had become one of the foremost issues and the heat dissipation efficiency is very poor in existing conventional cooling methods which leads to a rise in component temperature. Heat Pipes (HP) are extensively utilized to extract the heat, generated within the placed environment. Due to its compactness, these pipes can be used adequately in small/ confined spaces. The numerical and experimental research on the improvement of HP thermal performance by varying its factors such as heat flux, fluid filling ratio, working fluid, operating pressure, temperature, tilt angle, nanoparticles shape, and size of nanoparticles has been conducted by several authors [1–6].

Liu et al. [7] investigated the work of a miniature thermosiphon working with CNT/water nanofluid for a heat input range of 20–200 W. The result values recorded that a nanofluid of 0.8% could be the optimum volume fraction as the thermal resistance of the HP has been decreased. Santhisree et al. [8] worked experimentally on an eight-turn closed loop pulsating heat pipe by utilizing different operating fluids like acetone, methanol, ethanol, and water. The author considered the Taguchi technique to optimize the independent factors (heat load, fill ratio, tilt angle, and working fluid) of a CLPHP. The author observed that heat flux played an important role followed by tilt angle and filling ratio to enhance the thermal characteristics in terms of the thermal resistance (R). Gunnasegaran et al. [9] empirically studied about thermal characteristics of a loop heat pipe by passing Silica dioxide/water nanofluid with a 3.0% volume fraction by considering the heat inputs from 20W–100W

✉ Din Bandhu
din.bandhu@manipal.edu

1 Department of Mechanical Engineering, JNTU Ananthapur, Ananthapuramu, Andhra Pradesh, India

2 Department of Mechanical Engineering, G. Pulla Reddy Engineering College, Kurnool, Andhra Pradesh, India

3 Department of Mechanical Engineering, JNTUA College of Engineering, Anantapur, Andhra Pradesh, India

4 Department of Mechanical and Industrial Engineering, Manipal Institute of Technology Bengaluru, Manipal Academy of Higher Education, Manipal, Karnataka 576104, India

5 School of Mechanical Engineering, Lovely Professional University, Phagwara, Punjab 144001, India

Published online: 02 September 2023

and also compared with pure water. It is noted that thermal resistance is reduced to 28%—44% with nanofluid ranging mentioned heat loads. Features like rapid arrival of steady state and also lower evaporator wall temperature were also recognized. Tharayil et al. [10] analyzed experimentally and reported the heat transfer characteristics of miniature loop HP using graphene-distilled water nano-fluid. The diameter of the transport lines and evaporator were varied to prevent the reverse flow and increased the flow rate of condensed liquid. The results depicted that the graphene nano-particles with the volume concentration of 0.003% 0.006%, and 0.009% enhanced the thermal performance and also reduced the evaporator surface interface temperatures. It was lessened at about 10.3 °C for graphene nanofluid at 0.009% compared with distilled water. Senthilraja et al. [11] endorsed the method called a double step to prepare hybrid nanofluids (CuO, Al_2O_3-water) and mono (CuO-water, Al_2O_3-water) and experimentally computed the thermal conductivity (k) of said nano-fluids with volume concentrations, 0.2%, 0.1% and 0.05% at temperatures from 20^0 to 60^0C. The experimental results demonstrated that for 0.2% of particle volume concentration, an ultimate enrichment in thermal conductivity of 9.8% is been ascertained. Ramachandran et al. [12] conducted experiments with a 0.1% of volume fraction on a cylindrical mesh wick (capillary driven) HP with a heat load starting at 50 W and with an increment of 50 W up to 250 W at a horizontal position. The author utilized the hybrid nanofluid (water- CuO & Al_2O_3). It is observed that by using a hybrid nanofluid at 250 W the thermal resistance of 44.25% had been scaled down. Jafari et al. [13] investigated practically and analytically the heat transfer performance of HPs with a screen mesh. In order to decrease the thermal resistance an optimization approach is considered. Investigations were carried out on the orientation, evaporator, condenser lengths, and effect of the cooling temperature. It was constituted that permeability and the thickness of the wick are the active functions of the heat flux. Gupta et al. [14] carried out investigations experimentally and numerically to enhance the thermal performance of an HP using CeO_2–H_2O and water as the base fluid. In this way analyze the thermal performance of three different concentrations 0.5, 1.0, and 1.5 vol. %, and varying heat input like 10, 15, and 20 kWm^{-2}. The experimental and numerical outcome of a nanofluid showed that the thermal resistance and the temperatures of a heat pipe surface are diminished as compared with the base fluid (water). It is concluded that compared with water, CeO_2 /H_2O nanofluid has good heat transfer characteristics. Naresh [15] studied numerically a two-phase thermosyphon by considering water R134a as the operating fluid. To maximize the performance of a heat pipe arranged fins inside of a condenser with a length of 20 cm and varied fins from 0 to 8. For the input factors optimization purposes, a combined ANN and GA approach has been employed. Liu and Zhu [16] carried out experiments using CuO-H_2O nanofluid and pure water on a horizontal screen mesh wick heat pipe. The performance of a nanofluid is correlated with water and showed that contraction of 60% in the total thermal resistance of HP. Liu and Li [17] researched the studies on nanofluid with different heat pipes for the thermal performance enhancement in HPs with nano-fluid, and identified the following reasons; Brownian motion of nanoparticles, wettability, capillary action, number of active nucleation sites and increase heat pipe capillary force due to nanoparticles coating on wick surface, decline contact angle of solid–liquid, escalation in roughness, raise in effective thermal conductivity(k) of the nano-fluid were the dominant reasons attributed to the enrichment of heat transfer. Kole and Dey [18] demonstrated that intensification of 40% in thermal conductivity was evaluated using ZnO nanoparticles when suspended at 0.03% of volume fraction in EG base fluid. Asirvatham et al. [19] experimented with the heat transfer performance of mesh wick heat pipe using Ag-water nano-fluid with different volume fractions of 0.009, 0.006, and 0.003% at the heat load of 20–100 W. A Maximum of 76.2% cutback is found in thermal resistance and a decrement in evaporator surface temperature at all heat loads while using Nanofluid. Putra et al. [20] experimented on LHP (loop heat pipe) made of the collar (biomaterial) as wick using H_2O-Al_2O_3 as nanofluid with volume concentrations of 5%, 3%, and 1%. The authors noted that R (thermal resistance) and evaporator wall temperatures are curtailed at the volume fractions mentioned above in comparison to DI water. Kumaresan et al. [21] evaluated the thermal resistance using CuO/H_2O and DI water as nanofluid with sintered wick and screen mesh wick heat pipes with 1.5% and 0.5% volume fractions by varying the heat load from 10 W to 160 W. It was noted that surface temperature and thermal resistance were minimized by 27.08% and 49.64% respectively by using the sintered heat pipe and concluded as superior in thermal performance. Wan et al. [22] constructed an mLHP (miniature loop heat pipe) and compared the heat transfer characteristics using copper–water nano-fluid and DI water. A mass fraction of 1.0%–2.0% of Nanofluid was processed using SDBS (sodium dodecyl benzene sulfonate) surfactant in meager quantity with Cu nano-particles of size 50 nm. An ideal fraction of 1.5 wt% produced better thermal performance. Kim et al. [23] researched different shapes of alumina nanoparticles (Sphere, brick, and cylinder) that are suspended in acetone as the working fluid by a two-step method. As compared to base fluid sphere nanoparticles improve the thermal resistance by about 33%. Whereas cylinder and brick shape nanoparticles enhanced by 16% and 29% respectively. Mahdavi et al. [24] performed experimentation to evaluate the heat transfer performance of cylindrical HP with a mesh wick of copper material by considering two situations first as evaporator above condenser (gravity-opposed

orientations) and second as condenser located above evaporator (gravity-assisted orientations) by employing heat flux, tilt angle, and fluid fill volume. Experimentation was carried out in two scenarios the first is keeping an inclination angle which exhibited that the performance of HP was negligible. The second showcased that when increased in inclination angle the R was increased due to the difference in temperature between condenser and evaporator. Solomon et al. [25] researched the performance of heat pipe with cylindrical screen mesh (100 mesh-inch^{-1}) wick without and with deposition of copper nano-particles by varying three different heat inputs (250 W, 200 W, 150 W). The surface of the mesh is coated with nanoparticles with an average size of 80–90 nm. Results revealed lower thermal resistance and increased heat transfer coefficient at the evaporator section using coated mesh. Moraveji et al. [26] experimented with cylindrical sintered heat pipe considering a diameter of 8 mm, length of 190 mm, and wick thickness of 1 mm. The tested tube consisted of 90^0 curves in between the evaporator and condenser section with weight fractions of 0, 1, and 3 wt.%. Results found that the thermal resistance and wall temperature difference were decreased and efficiency increased at 3 wt.% nanofluids (Al_2O_3) when compared with water. Reddy et al. [27] studied the input parameters of a wick HP as heat flux, nanofluid concentration, and tilt angle. Adopting RSM methodology optimized the input variables. Sarafraz et al. [28] researched to quantify the thermal resistance and heat transfer coefficient by constructing a thermosyphon heat pipe of copper to perform to a maximum of 200 kwm^{-2} of heat flux by preparing the nanofluid with acetone and zirconia. It has evident that the thermal resistance of the HP declined to minimal when more heat load is applied at the evaporator and the heat transfer coefficient of the evaporator is also elevated. Khajehpour et al. [29] researched using nanofluids (SiO_2/H_2O) to calculate the thermal performance in terms of R (thermal resistance) on L-shaped heat pipe at a heat load of 15 W, 10 W, and 5 W. It was noted that decrement in R by an increase in nano-fluid concentration and also with the angle of reduction. When correlated with water, a reduction in R of 24% was noted at a heat input of 10 W, nanoparticles dimension of 11–14 nm, a concentration of 0.5 wt.%, and inclination of 90^0. It had been concluded that there is an escalation in thermal resistance due to an increase in the size of nanoparticles. Khajehpour et al. [30] determine the enact of working parameters of load on the engine, engine speed, and blended levels of ethanol in diesel fuel (biodiesel) on the engine emission characteristics (NOx, CO, and CO_2) of DI diesel engine. The DOE tool is used to evaluate the experimentation on RSM-based Central composite rotatable (CCD) design. Reddy et al. [31] reviewed that in order to transfer extensive heat, a heat pipe would be one of the better heat transfer devices due to its uncomplicated structure and processing good reliability. Working fluid has a predominant role depending on its conductivity due to the nature of its conductivity. In order to decrement the resistance, and improve the thermal efficiency and heat transfer coefficient, oscillating heat pipes and heat pipes will play a major role. It is being targeted at replacing the nano-fluids over the traditional fluids which are to be used in the heat pipes. Gunnasegaran et al. [32] presented the results of conducted experiments using PC-PCU cooling on loop heat pipe (LHP). Pure water with three different concentrations (0.5, 1.0, 3.0 wt. %) of silica nanoparticles (SiO_2) is considered nanofluid. Response Surface Methodology has been opted for optimization of the input parameters (mass concentration and heat input) and output parameters (thermal resistance) of an HP. They analyzed that TR has been decreased up to 0.5% and increased thereafter and found the optimized values are with a heat load of 59.97 W and 0.48 vol. % concentration.

Vidhya et al. [33] studied, hybrid Al_2O_3 and SiO_2 nanoparticles with a W/EG binary mixture are used to improve the heat transmission properties of cylindrical screen mesh heat pipes. The heat transfer capacity was shown to improve with hybrid nanofluid volume concentration and heat input power, according to the experimental results. Beiginaloo et al. [34] conducted experiments on a thermosyphon heat pipe and optimized using CFD and DOE. The optimal values for aspect ratio, heat load, and filling ratio were obtained in this regard. The CFD simulation's results and the experimental data had a respectable level of agreement. Adin et al. [35–39] conducted an experimental investigation into the effects of Total Accumulated Weld Volumes (TAWV) and various groove angles (45°, 60°, 75°, and 90°) on the mechanical characteristics of AISI 1040 and AISI 8620 cylindrical steel joints. Scanning electron microscopy (SEM) was also used to evaluate the sample fracture surfaces.

From the literature review, it can be implied that RSM can be a better-designed tool for operational parameters for optimization purposes of the HP independent variables. It also depicted an escalation in the heat transfer performance of the HP using different concentrations of water-based nanofluids. The appropriate selection of basic fluids is mostly determined by the technical area of concern. Oil-based nanofluids, for example, are typically utilized in manufacturing processes for lubricating or high-temperature applications, whereas water and ethylene glycol-based nanofluids are regularly used in regions where the fluid is used for cooling purposes in various pipelines or channels. Despite the fact that ethylene glycol's thermal conductivity is lower than that of water. The novelty of this study is, the water-based alumina liquids are charged into cylindrical screen-mesh heat pipes at varying volume concentrations: 0.05%, 0.15%, 0.25%, at moderate heat inputs of 100, 150, and 200 W and tilt angles 0, 45 and 90^0. The relationship between dependent and independent

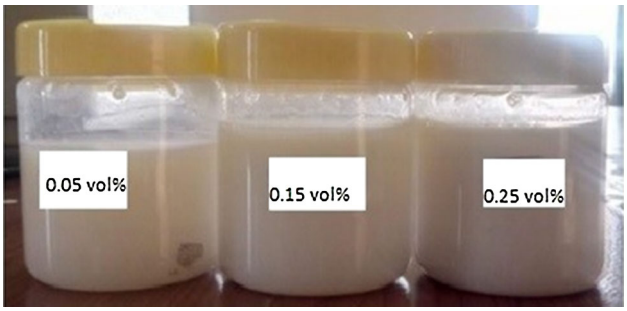

Fig. 1 Prepared Al_2O_3 –DI water nano-fluids

variables was examined using the response surface methodology and the ANOVA tool. For the assessment of thermal resistance in addition to thermal conductivity, which is not frequently noted in the literature, new regression correlations were built using the experimental results.

2 Materials and methods

2.1 *preparation of* Al_2O_3 *nanofluid sample*

The alumina (Al_2O_3) nanoparticles (99.8% pure, 3980 kg/m^3, spherical, and < 50 nm) used in this study were manufactured by PlasmaChem GmbH, Germany. A double-step technique is utilized to prepare DI water-alumina nano-fluid. Initially, nano-particles were dispersed in DI water without any surfactant. After that, the mixture (water and nanoparticles) is kept in an ultrasonicator [Hielscher, UP400S,] at 50–60 kHz frequency for 60 min to ensure that the solution is evenly distributed and good stability is achieved. The current experimental work considers the impact of nanoparticle volume fraction (ø) concentration (0.05, 0.15, and 0.25 Vol. %) calculated using Eq. 1 [27], and the prepared water/alumina nanofluids were shown in Fig. 1. In this approach, it has been found that 1.98, 5.97, and 9.95 mg, respectively, of alumina nanopowder are needed to prepare 0.05, 0.15, and 0.25 vol.% concentrations.

The zeta potential is the difference in potential between the dispersion medium and stationary fluid layer that is associated with the dispersed particle. Zeta potential value indicates the strength of the attraction between neighboring, comparable charged particles in a dispersion. High (negative or positive) zeta potential solutions indicate strong attraction between the particles. Therefore, the colloidal solution is electrically stabilized since the particles do not aggregate. In general, the stability of nanoparticles with zeta potential values larger than + 25 mV or less than − 25 mV is very high. The Zeta potential test was performed by Zetasizer to ensure the stability of the nanofluid and is shown in Fig. 2.The value for the sample given as + 31 mV (it is assumed that a value above ± 25 mV has good electro-static stability). This implies that the prepared sample quality is good and stable [15].

$$\%\ \text{volume fraction}\ (\text{ø}) = \frac{\frac{W_n}{\rho_n}}{\frac{W_n}{\rho_n} + \frac{W_b}{\rho_b}} \tag{1}$$

where w_b, ρ_b, w_n, and ρ_n are the weight, the density of water, weight and density of nanoparticles respectively.

2.2 *Characterization of* Al_2O_3*nanoparticles*

By X-ray diffraction method using Shimadzu LabX-6000, the crystalline phase of alumina nanoparticles was determined. The XRD picture outlined in Fig. 3 and the crystalline nature of the nanoparticle is also observed. Using the Scherrer formula below, the mean crystalline size of the alumina nanoparticle was determined [6].

$$D_c = \frac{K\lambda}{\beta \cos 2\theta} \tag{2}$$

In the above equation, λ is the X-ray wavelength (1.54056 A^0), D_c represents the crystalline size in nm and K is the shape (0.9–1.2) factor and the maximum intensity corresponding to 2θ was found to be 43.22 (Fig. 3). It was found that the β from the XRD data process sheet was 0.27 and the average size of aluminium oxide was found to be 28.46 nm based on the calculation. By using SEM (scanning electron microscope) analysis further the alumina nanoparticles dispersion was characterized. Figure 4 shows a 0.15 vol. % concentration SEM image of alumina nanoparticles at 40,000X magnification. The size of alumina nano-particles has been found to range from 23 to 34 nm in some locations and to be less than 50 nm.

2.3 Heat pipe construction and experimental procedure

Figure 5 depicts the schematic illustration of the HP experimental setup. It comprises the temperature control unit, auto transformer, data logger, digital multimeter, and a personal desktop. Heat pipes were prepared using traditionally available copper tubes which consist of 3 different sections; evaporator (10 cm), adiabatic (5 cm), and condenser (15 cm) section. The dimensions of the heat pipe which were considered are total length, inner diameter, outer diameter and thickness of the HPs are 30 cm, 1.15 cm, 1.27 cm, and 0.06 cm respectively. The wrapping was done for the inner surface of the HP to fix it securely by using a mechanism that consists

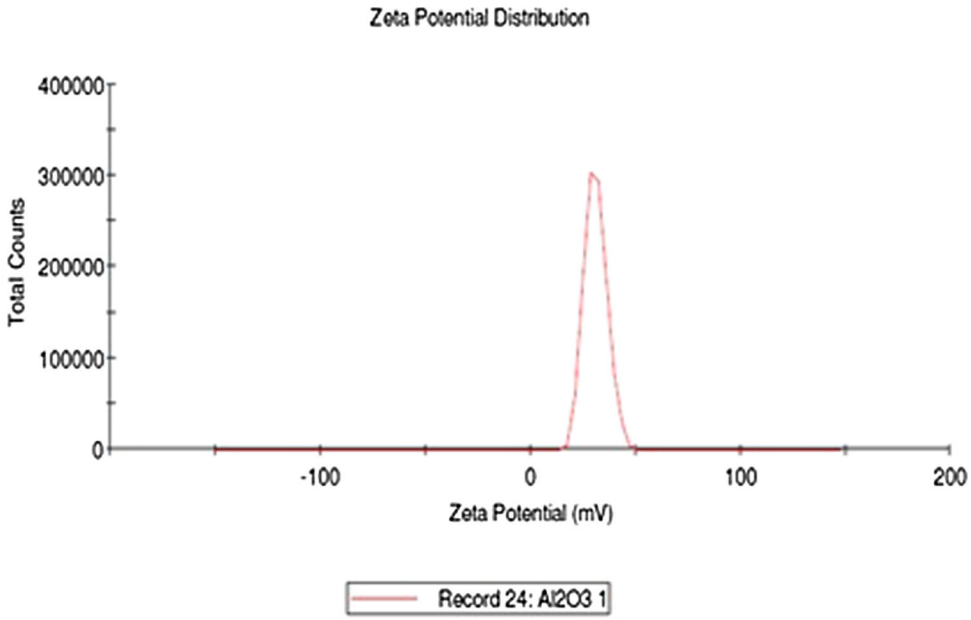

Fig. 2 Zeta potential analysis of Al_2O_3/DI water

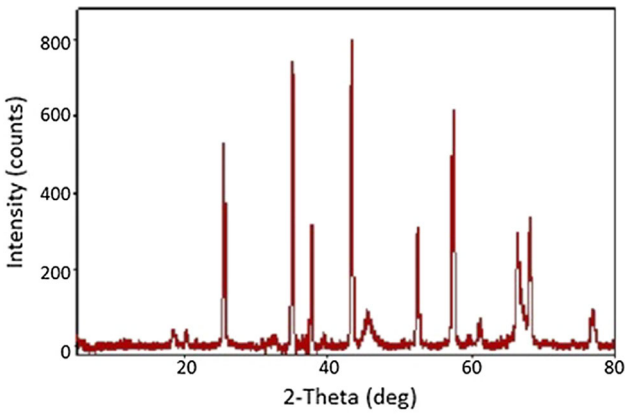

Fig. 3 XRD pattern of Al_2O_3 nano-particles

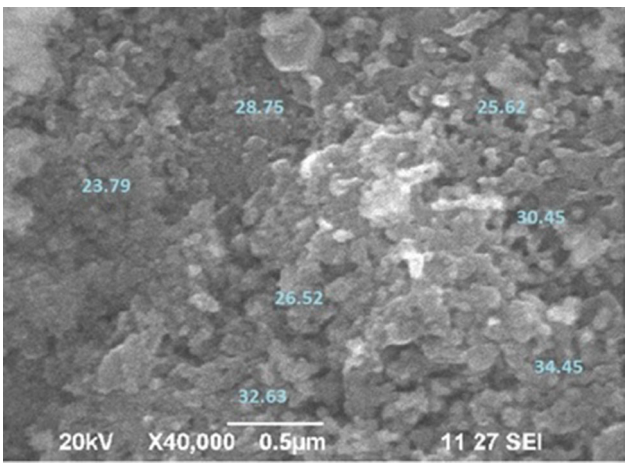

Fig. 4 SEM image of Al_2O_3 nano-particles

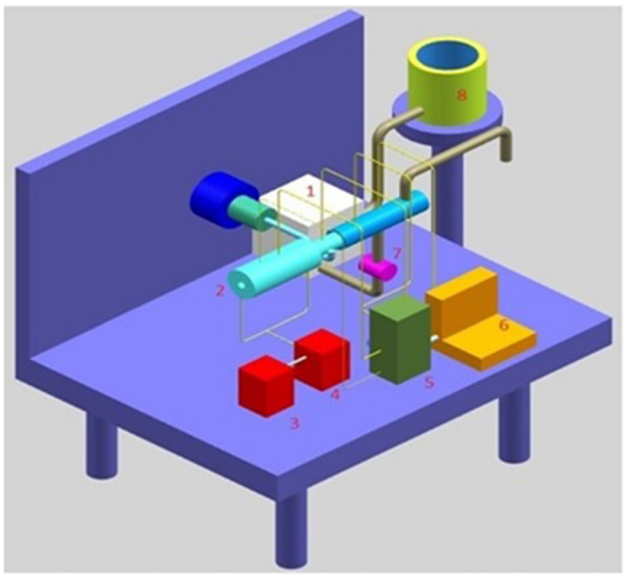

Fig. 5 Schematic diagram of HP test facility

of three layers of copper mesh wick with a wire diameter of 0.015 cm and mesh number 100 inch^{-1} connected by a spring and caps were used to close both ends of the copper tubes. In order to remove the gasses which are present in the HP, a vacuum pumping system (Model VS 65D, Hindhivac) at a pressure of 1×10^{-4} m bar was used to fill 30% of the total volume of the heat pipe charged with working fluid based on the earlier investigations [28]. A nichrome wire heater is wounded on the outer surface of the evaporator by giving a

230 V/50 Hz AC as a heat input. An autotransformer regulated the power supply to the electric heater, and the power input was measured with a digital multimeter. The evaporator and adiabatic zones of the heat pipes were completely insulated with glass wool to reduce heat loss.

An acrylic pipe with a diameter of 30 mm was utilized to cover the condenser portion of the HP and water is used as a coolant which extracts heat from the heat pipe. The HP test set-up also consists of a flowmeter and a pump to circulate cooling water through the condenser segment at a steady flow rate of 15 l/h. In order to obtain the accuracy of results, the constant temperature of the water bath has been used to maintain the inlet temperature of the circulating water at 20^0 C for all test HPs of various heat inputs. A sum of five thermocouples of T-type with an uncertainty of $\pm 0.5^0$ C was fixed along the test area (one in adiabatic, two in evaporator, and two in condenser zone) are illustrated in Fig. 6. The given heat loads were 100 W, 150 W, 200 W and orientations for all the heat pipes are 0^0, 45^0 and 90^0. Every experiment was conducted until a constant surface temperature of the heat pipe was shown by the thermocouples.

Figure 7 displays measuring the thickness of the screen wire mesh which was inserted in the heat pipe. The wick structure ε(porosity) and K permeability were evaluated using Eqns. 3 & 4 [19] and found to be 0.76 and 3.98 × 10^{-10} m^2 respectively.

$$\varepsilon = 1 - \frac{\pi SNd}{4} \tag{3}$$

$$K = \frac{d^2}{122}\frac{\varepsilon^3}{(1-\varepsilon)^2} \tag{4}$$

2.4 Thermal analysis of an HP

The thermal resistance (R) of a heat pipe is directly proportional to the difference in temperature of the evaporator section and condenser section; and inversely proportional to the heat load, also be expressed as [13]:

$$R = \frac{T_e - T_c}{Q} \tag{5}$$

$$Q = VI \tag{6}$$

where T_c ($T_c = (T_{c1} + T_{c2})/2$) and T_e ($T_e = (T_{e1} + T_{e2})/2$) are condensers and evaporator surface average temperatures, respectively. The thermal conductivity (k) of a heat pipe is determined by the following formulae [27]:

$$k = \frac{L_{ef}}{A_{cs}R} \tag{7}$$

where R, A_{cs}, and L_{ef} are thermal resistance, cross-section area, and effective length of the heat pipe, respectively.

$$L_{ef} = 0.5L_e + L_a + 0.5L_c \tag{8}$$

where L_a, L_c, L_e adiabatic, condenser, and evaporator sections length respectively.

2.5 Response surface methodology (RSM)

The cylindrical screen mesh wick heat pipe input parameters were optimized by RSM using Minitab 17. The 3-level and 3-factor Box Behnken Design (BBD) has been employed in this work with 15 experiments. Three identified input variables are A: heat load (100–200 W); B: tilt angle ($0–90^0$); C: concentration of nanofluid (0.05–0.25 vol.%). The levels of each input variable have been chosen based on previous studies. The variables are coded as low (− 1) or high (+ 1). When examining the limitations of nanofluid, it was discovered that as the concentration of the fluids increased, so did their density, necessitating more pumping force to circulate the nanofluid in the heat pipe. As density grows as a result of an increase in nanofluid concentration, ineffective results are produced. In order to ensure that the task can be done successfully and with good results, the levels of nanofluids are maintained within the limitations. In many scientific experiments using RSM, researchers choose three evenly spaced levels. As a result, the Box Behnken design offers a viable and valuable alternative to the central composite design. As we can see from the sample sizes, there is enough information to test for lack of fit. The Box Behnken design does not vary significantly from rotatability. Another distinguishing feature of the BBD is its spherical shape [40]. Table 1 shows the complete BBD design matrix in terms of input factors. According to the viability and applicability in the sectors, the lower and higher limits of the elements are taken into consideration. The study included 15 experiments, and the correlation between dependent and independent variables was established. The response from these independent variables was taken as 'R' and 'k' of the heat pipe. The practical data obtained by the above procedure were analyzed using regression Eq. (9).

$$Y = b_0 + \sum_{k=1}^{n} b_k x_k + \sum_{k=1}^{n} b_{kk} x_k^2 + \sum_{k=1}^{n-1}\sum_{m>k}^{n} b_{km} x_k x_m + e \tag{9}$$

where Y is the heat pipe response factor, b_o, b_k, b_{kk}, and b_{km} are intercept term, linear, quadratic, and interaction coefficient. x_k and x_m are coded independent variables, k is the number factors and e is the random number [3].

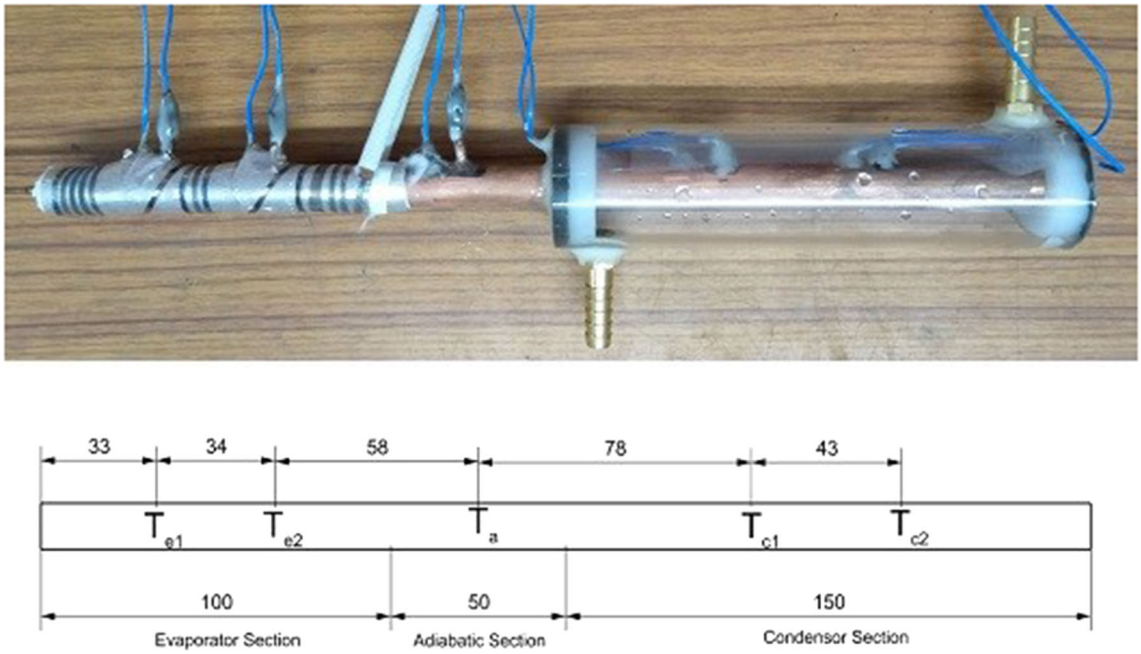

Fig. 6 Schematic of the test section

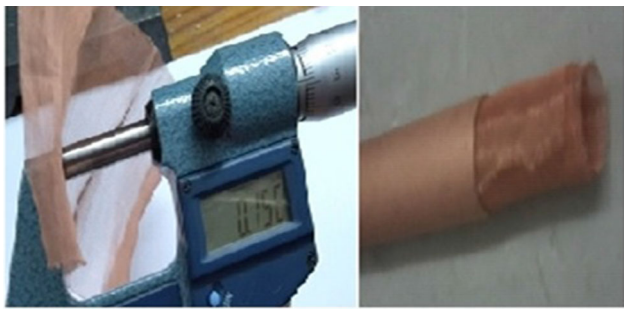

Fig. 7 Images of the screen mesh and HP

3 Results and discussion

3.1 Box behnken design model and statistical analysis

Experimental work was carried out using the BBD approach to determine the best reaction conditions for minimizing 'R' and maximizing 'k' of a wick heat pipe and to study the effect of input parameters on responses. Table 2 depicts the responses obtained from various parameter combinations. The following are the mathematical model equations (Eqs. 10 and 11) derived from the predicted values of the output parameter (R and k) in terms of the coded variables:

$$\begin{aligned} R = {} & 0.20943 - 0.000075A - 0.000733B \\ & - 0.4139C - 0.000000A * A + 0.000006B * \\ & B + 1.2021C * C + 0.000001A * B \\ & - 0.000070A * C + 0.000074B * C \end{aligned} \tag{10}$$

$$\begin{aligned} k = {} & 5807 + 8.31A + 42.21B + 24326C \\ & - 0.00031A * A - 0.35301B * B - 74682C * C \\ & - 0.02649A * B + 10.19A * C + 1.80B * C \end{aligned} \tag{11}$$

3.2 Analysis of variance (ANOVA)

Table 3 shows the results of ANOVA performed to determine the significance by F-test and fitness of the quadratic model, as well as the impact of significant individual terms and their

Table 1 HP input factors and their levels

Symbols	Factors	Units	Level-1	Level 0	Level 1
A	Heat input	W	100	150	200
B	Inclination	Deg	0	45	90
C	Concentration	Vol. %	0.05	0.15	0.25

Table 2 Arrangement of Box Behnken design and responses of a heat pipe

Expt. no	Heat load (W)	Tilt angle (^{0})	Concentration (Vol.%)	Thermal resistance ($^0CW^{-1}$)	Effective Thermal conductivity (Wm^{-1} K^{-1})
1	200	90	0.15	0.1394	10,230.47
2	200	45	0.25	0.1383	10,311.84
3	150	45	0.15	0.1390	10,262.99
4	100	45	0.25	0.1517	9402.295
5	150	90	0.05	0.1631	8744.440
6	150	45	0.15	0.1390	10,262.99
7	100	45	0.05	0.1617	8820.797
8	100	90	0.15	0.1510	9445.884
9	200	0	0.15	0.1460	9768.034
10	100	0	0.15	0.1631	8745.077
11	150	0	0.05	0.1754	8129.697
12	150	45	0.15	0.1390	10,262.99
13	200	45	0.05	0.1497	9526.625
14	150	0	0.25	0.1613	8842.020
15	150	90	0.25	0.1503	9489.128

interaction on the selected responses 'R' and 'k'. The F-test has been used to manage the statistical significance of Eqs. 10 and 11. Model terms are significant when the *p* (probability) > F is less than 0.05. If the value is more than 0.05, the model terms are not significant. The lower the p-value, the greater the significance of the corresponding coefficient [41–44].

Independent variables that had a significant influence on heat pipe responses (R and k) were heat input (A), heat pipe inclination (B), and nanofluid concentration (C), and interaction terms were observed between the main factors (AB for R and AB, AC for k), while significant quadratic terms were B^2 and C^2. The model's F-value of 131.18 for 'R' and 561.61 for 'k' with a p-value of 0.000 indicates that the model is significant, at a 95% confidence level. The greater the significance of the corresponding coefficient, the lower the p-value [2].

The RSM's feasibility is also ensured by observing the statistical (s) value of both 'R' and 'k' of an HP which were found to be 0.00125 and 37.016, respectively. Similarly, the coefficient of determination (R^2) was found to be 99.58% and 99.90%, respectively. R^2 (adj) values for considered responses are 98.82% and 99.72%, respectively. The R^2 value of both responses 'R' and 'k' was found to be satisfactory, as it was greater than 95%.

3.3 Interaction effects of the input factors on responses

The interaction effects of the three considered input parameters of the HP on its heat transfer performance were studied using contour or surface plots. The contour plots for both thermal resistance (R) and thermal conductivity (k) were developed with three different considered input variables using Minitab–17. The contour plot was generated to show the effect of two different input factors on the response variable withholding the third factor.

Figure 8 depicts the contour plot of 'R' with respect to the input parameters (A, B, and C). The surface plot of 'R' with respect to heat input and concentration of nano-fluid by holding the B value at 52^0 is shown in Fig. 8a. From the image it was observed that the better 'R' can be obtained at C limits of 0.12 Vol. % – 0.22 Vol. % and factor A limits of 170–200 W. Figure 8b shows the contour plot of 'R' with respect to nanofluid concentration and inclination by holding the factor A at 200 W. From the picture, it was observed that the better 'R' can be obtained at C limits of 0.12 Vol. % – 0.22 Vol. % and B limits of 25^0–75^0. Figure 8c shows the contour plot of 'R' with respect to heat load and tilt angle by holding C at 0.177 Vol.%. From the picture, it was observed that the better 'R' can be obtained at A limits of 170–200 W and B limits of 25^0–75^0.

The contour plots of "k" with respect to the input variables are shown in Fig. 9. Figure 9a depicts the contour plot of "k" with respect to heat input and concentration of nanofluid when the B value is held constant at 52^0. According to the image, the best "k" can be obtained at C limits of 0.12–0.22 Vol.% and A limits of 170–200 W. By keeping A at 200 W, the contour plot of "k" with respect to nanofluid concentration and tilt angle is shown in Fig. 9b. According to this, the best "k" can be obtained at C limits of 0.12–0.22 Vol.% and B limits of 25 – 75^0. Figure 9c depicts the contour plot

Table 3 ANOVA of the mesh wick HP input parameters

Source	Thermal Resistance- 'R'					Thermal Conductivity- 'k'				
	DF	Adj-SS	Adj-MS	F-value	*P*-value	DF	Adj-SS	Adj-MS	F-value	*P*-value
Model	9	0.001859	0.000207	131.18	0.000	9	6,925,869	769,541	561.61	0.000
Linear	3	0.000878	0.000293	185.81	0.000	3	3,196,353	1,065,451	777.57	0.000
A	1	0.000365	0.000365	231.68	0.000	1	1,464,542	1,464,542	1068.83	0.000
B	1	0.000221	0.000221	140.28	0.000	1	735,136	735,136	536.50	0.000
C	1	0.000292	0.000292	185.48	0.000	1	996,675	996,675	727.38	0.000
Square	3	0.000973	0.000324	205.94	0.000	3	3,704,675	1,234,892	901.23	0.000
A*A	1	0.000002	0.000002	0.96	0.373	1	2	2	0.00	0.969
B*B	1	0.000492	0.000492	312.63	0.000	1	1,886,786	1,886,786	1376.98	0.000
C*C	1	0.000534	0.000534	338.89	0.000	1	2,059,375	2,059,375	1502.94	0.000
2-Way Interaction	3	0.000008	0.000003	1.80	0.264	3	24,842	8281	6.04	0.041
A*B	1	0.000008	0.000008	4.80	0.080	1	14,205	14,205	10.37	0.023
A*C	1	0.000000	0.000000	0.31	0.601	1	10,375	10,375	7.57	0.040
B*C	1	0.000000	0.000000	0.28	0.618	1	262	262	0.19	0.680
Error	5	0.000008	0.000002			5	6851	1370		
Lack-of-Fit	3	0.000008	0.000003			3	6851	2284		
Pure Error	2	0.000000				2	0	0		
Total	14	0.001867	0.000000			14	6,932,721			
	Summary of the model					Summary of the model				
	S—0.001254		R^2—99.58%			S—37.0167		R^2—99.90%		
	R^2-adj—98.82%		R^2-pred—93.25%			R^2-adj—99.72%		R^2-pred—98.42%		

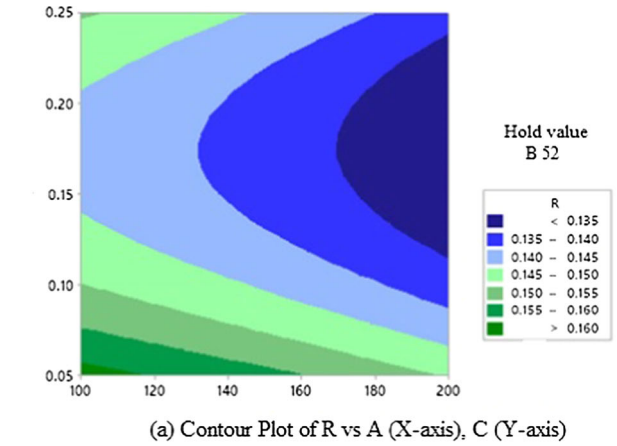

(a) Contour Plot of R vs A (X-axis), C (Y-axis)

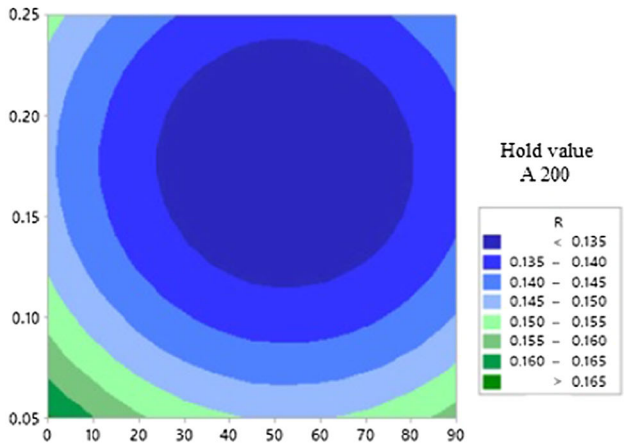

(b) Contour Plot of R vs B (X-axis), C (Y-axis)

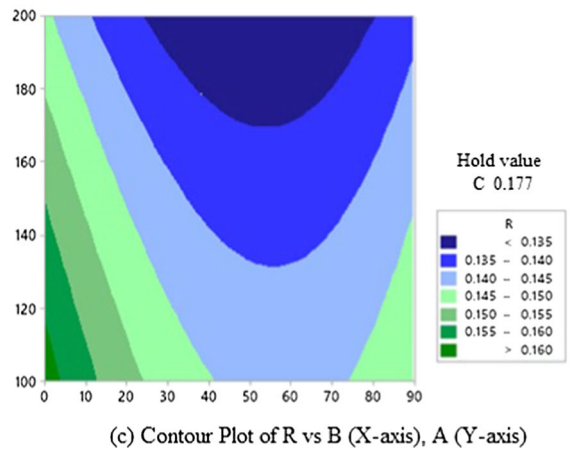

(c) Contour Plot of R vs B (X-axis), A (Y-axis)

Fig. 8 Contour plots of response 'R' of an HP

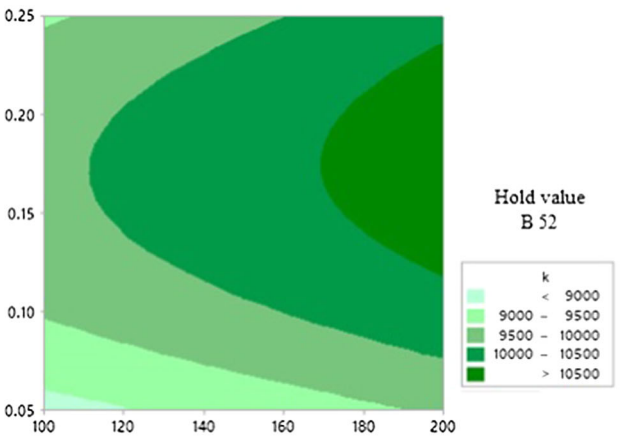

(a) Contour Plot of k vs A (X-ais), C (Y-axis)

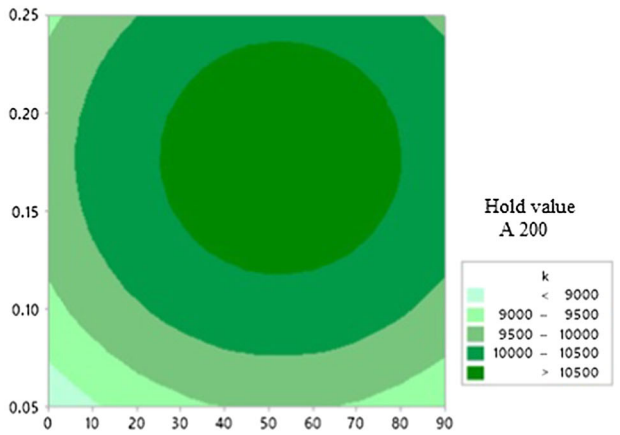

(b) Contour Plot of k vs B (X-axis), C (Y-axis)

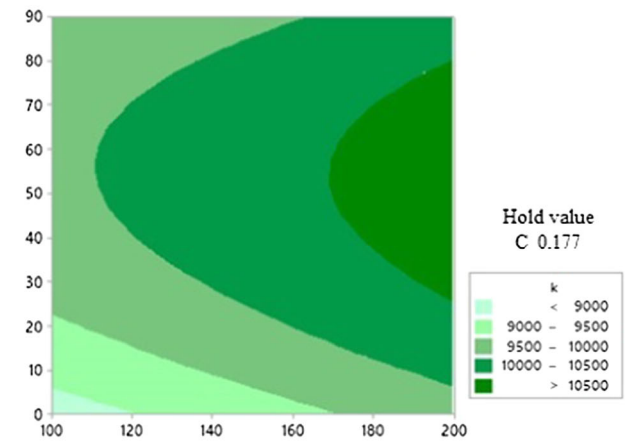

(c) Contour Plot of k vs A (X-axis), B (Y-axis)

Fig. 9 Contour plots of 'k' of an HP

of "k" with respect to heat load and tilt angle when C is set to 0.177 Vol.%. According to the picture, the best "k" can be obtained at A limits of 170–200 W and B limits of 25–75^0.

According to the contour plots, 'R' decreases as the heat input increases, implying that it is high at lower heat flux and low at higher heat flux. This is due to the fact that the surface tension between solid–liquid interfaces is high at low heat flux and decreases as heat input increases. The film thickness of the liquid layer is also high at low heat inputs. This results in high heat resistance, but as the heat input increases, the film thickness decreases. Whereas for inclination, the 'R' decreases up to a certain point and then increases as the input factor levels increase. This is because the large inclination angle allows the liquid to quickly return from the condenser to the evaporation section, but the vapors production in the evaporator is insufficient. Thermal resistance is reduced with increasing nanofluid concentration up to a certain limit, after which it increases due to the thermos-physical properties of nanofluids namely viscosity, density, and fluid flow resistance. Thermal conductivity is the inverse of thermal resistance [15, 45].

3.4 Model accuracy check

An accuracy check is required to obtain an adequate model. The accuracy of the model was tested by comparing experimental and predicted thermal resistance and thermal conductivity response values. The regression coefficient (R^2) was used as a basis of comparison, with $R^2 = 99.58, 99.90\%$ for 'R' and 'k', indicating that the predicted values of responses matched the experimental values well. The scattered plot of "k" between experimental and predicted results is shown in Fig. 10 and the points are almost in line with the regression line, and concludes that the predictive capability is high [29]. The developed model can successfully predict responses for various factors combined within the specified limits of the input parameters. Similarly, Fig. 11 depicts the scattered plot of "k" between predicted and experimental values and it confirms that the prediction capability is high since the points are nearly in line with the regression line.

3.5 Mesh wick condition after utilizing alumina nano-fluids

After performing the experiments, an SEM (JSM 6300 model microscope, JEOL USA) photograph of the plain wick and the one with alumina nanoparticles was acquired in order to compare the porous coating layer formation, caused by the addition of nanoparticles in the mesh wick surface of the evaporator zone [6, 21]. The SEM photograph of the mesh wick surface without consisting of nano-particles is shown in Fig. 12a. The wall of the wick surface is found to be smooth, as can be seen in the image. However, the SEM view of the wick surface with 0.15 vol.% of Al_2O_3-water nano-fluids is shown in Fig. 12b. The porous coating layer made of alumina nano-particles is evidently present on the wick surface. This finding serves as proof that a thin porous coating layer formed at the evaporation section's screen mesh wick. High heat transfer rates occur if the coating layer on the mesh wick surface provides an extra evaporating surface. This significantly lowers the heat pipe's 'R' and improves the capillary pumping capacity needed to draw liquid to the evaporator region from the condenser section [27, 44]. As a result, the heat pipe's heat transfer rate is increased while utilizing the alumina-water nanofluid.

3.6 Optimized responses of a screen mesh wick HP and confirmation tests

The first response of a mesh wick heat pipe, thermal resistance (R) has to be minimized and the second response thermal conductivity (k) has to be maximized. RSM optimizer has been employed in a Minitab 17 program, to find the optimum HP input parameters for the best possible HP responses as shown in Figs. 13 and 14.

Figure 13 depicts the thermal resistance optimum input variables plot. A heat input of 200 W, an inclination angle of 52.72^0, and a concentration of 0.1773 Vol.% are the optimum limits of the three input parameters. At these parameter settings, the thermal resistance was predicted, and the response (R) value was found to be 0.1304 ^{0}C W^{-1}. As seen from the figure, the 'R' decreases as the heat input increases, whereas for the inclination angle and concentration of nano-fluid, the 'R' decreases up to a certain limit and then increases after increasing the input variable levels.

The optimization plot for thermal conductivity is shown in Fig. 14. The 'k' was predicted at the optimum input parameter settings, and the response(k) value was 10,770 W m^{-1} K^{-1}. From Fig. 14, it is observed that the thermal conductivity increases with increasing heat input, whereas tilt angle and nanofluid concentration, increased up to a certain limit and decreased further, after increasing the input variable levels.

The model equations have been used to find the HPs optimum 'R' and 'k'. A set of three experiments were conducted with different input conditions chosen from a range of variables to validate the suggested model. As a result, the experimentally obtained values are rather close to the theoretically estimated data offered by the suggested models. The difference between experimental and predicted values was found to be around 5%. The developed model's predictive capability is significantly higher due to the lower error percentage between predicted and experimental results shown in Table 4.

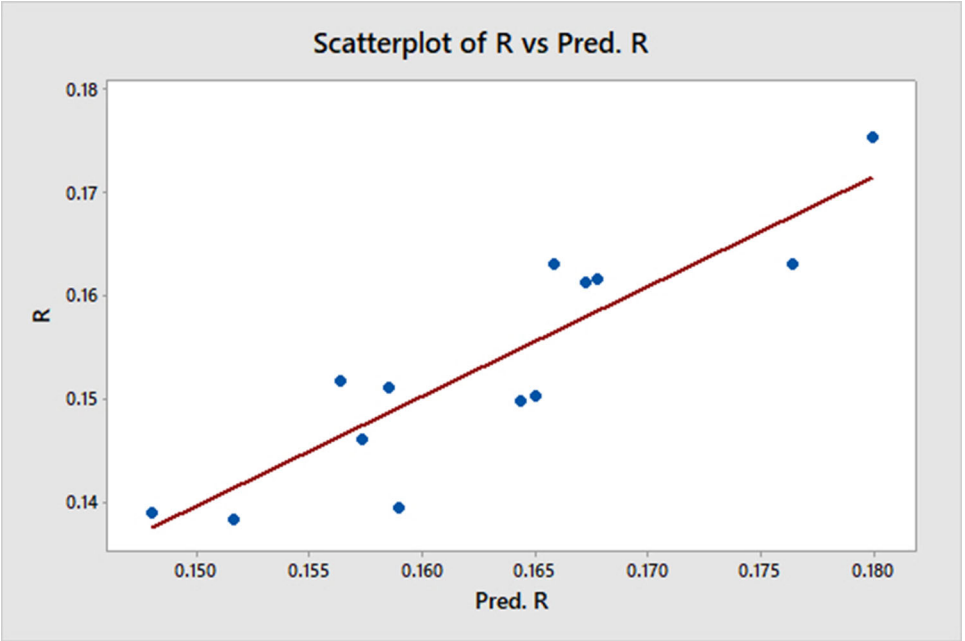

Fig. 10 Experimental vs Predicted plot of 'R'

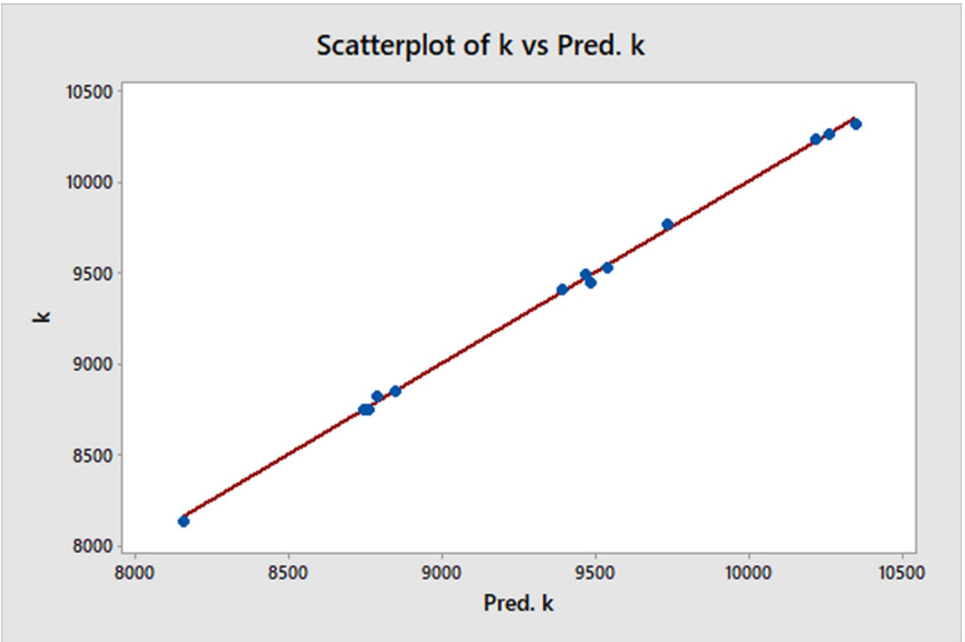

Fig. 11 Experimental vs Predicted plot of 'k'

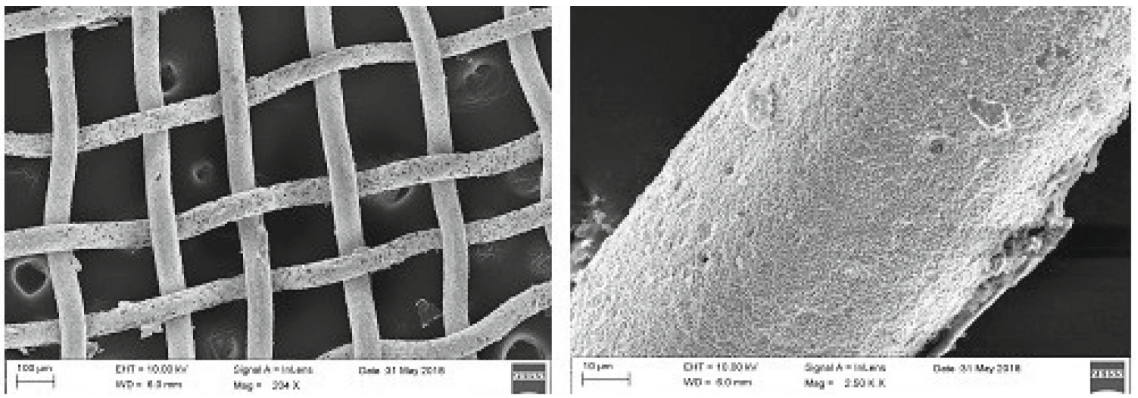

(a) Smooth surface before experimentation

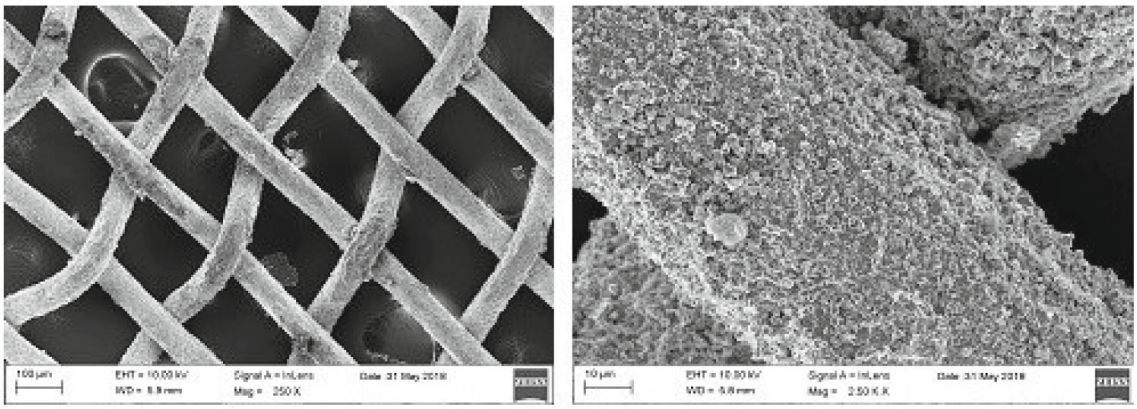

(b) Rough surface after experimentation

Fig. 12 Surface morphology of the wick surface

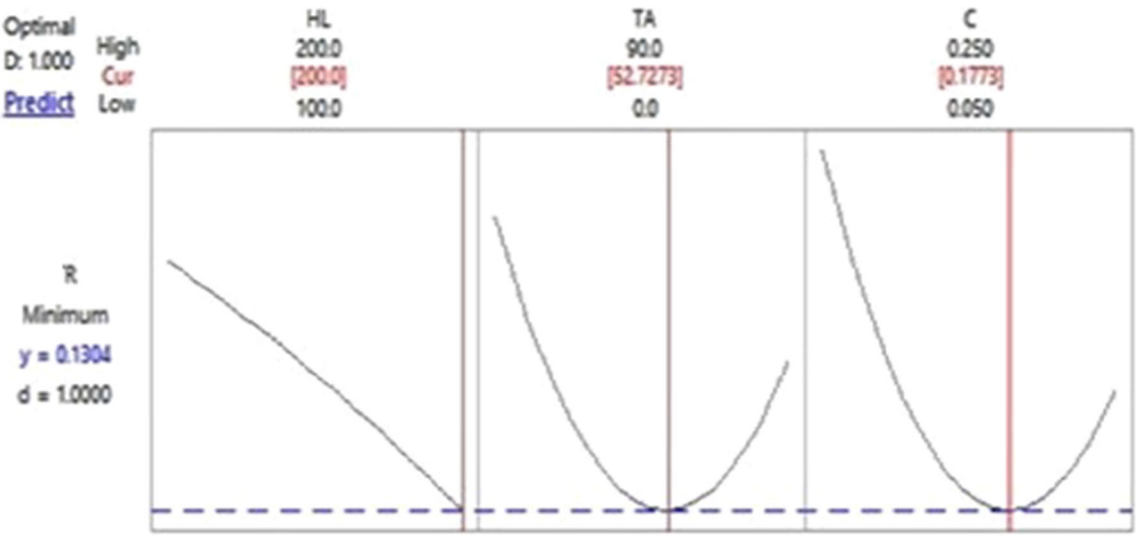

Fig. 13 Response optimization of 'R'

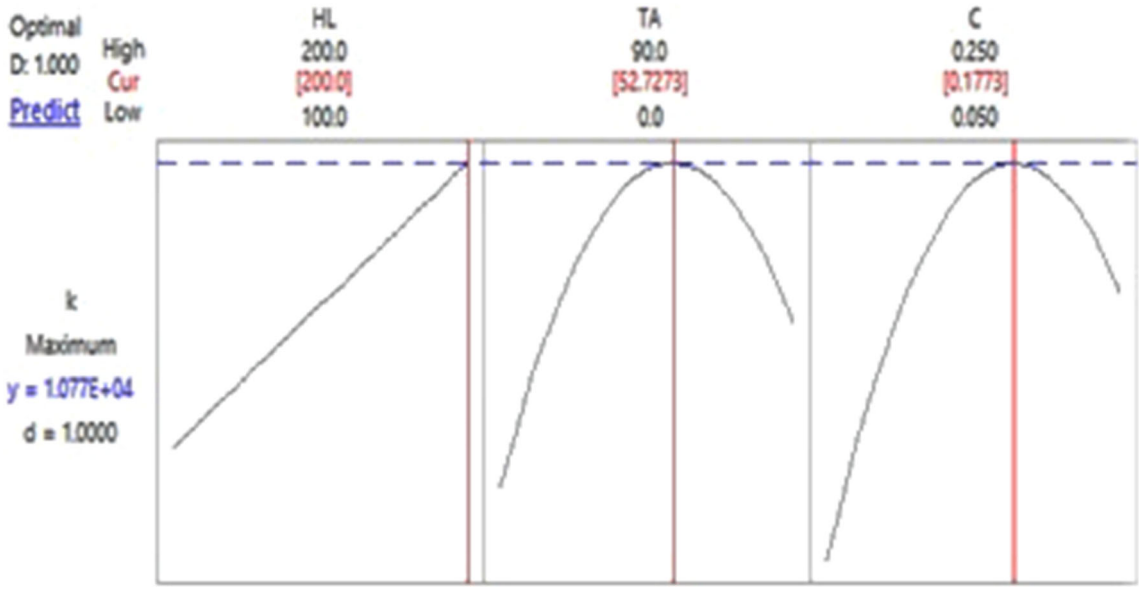

Fig. 14 Response optimization of 'k'

Table 4 Confirmation tests

Input factor settings			R (^{0}CW^{-1})			k (Wm^{-1} K^{-1})		
A (W)	B (^{o})	C (vol. %)	Pred	Expt	Error (%)	Pred	Expt	Error (%)
200	50	0.17	0.1454	0.1534	5.51	10,758	10,502	2.37
200	60	0.20	0.1474	0.1399	5.08	10,707	10,547	1.49
200	55	0.15	0.1467	0.1522	3.74	10,708	10,454	2.37

4 Conclusions

The following conclusions were reached after conducting several tests on a cylindrical screen mesh wick HP while varying the heat input, inclination, and volume fraction (concentration) of alumina nanofluids at various levels concurrently:

1. The Design of Experiments (DOE) based on response surface methodology (RSM) was extremely useful in designing the HP experiments, and statistical analysis assisted in identifying the significant parameters that have the greatest influence on the thermal characteristics of a mesh wick heat pipe. This experiment design significantly reduced the time needed by decreasing the number of experiments required and represented statistically proven models for all responses.
2. The parameter influence and empirical models were developed using statistical methods such as regression analysis and response surface approach. According to the ANOVA table, the independent variables that influence thermal resistance and thermal conductivity are volume concentration, tilt angle, and power are the significant input parameters that affect the heat transfer performance of heat pipe. The obtained thermal resistance and thermal conductivity response values are extremely close to one another, indicating the accuracy of the RSM models that were developed.
3. In the present investigation, the desirability approach of RSM was found to be the simplest and most efficient optimization technique. At a heat load of 200 W, an inclination angle of 52^0, and a nano-fluid concentration of 0.17 Vol.%, a high desirability of 95% was obtained. This condition was deemed to have the best parameters for the heat pipe, with an 'R' of 0.1304 ^{0} C W^{-1} and a 'k' of 10,770 W m^{-1} K^{-1}.
4. The porous coating layer formed on the wick surface at the evaporator section was observed from SEM analysis, which produces good capillary structures which increase wettability and the heat transfer area, which may be the main reason for the thermal performance improvement of HPs with alumina nano-fluids.

Funding Open access funding provided by Manipal Academy of Higher Education, Manipal.

Data availability The authors confirm that the data supporting the findings of this study are available within the article.

Declarations

Conflict of interest The authors declare no conflict of interest.

Open Access This article is licensed under a Creative Commons Attribution 4.0 International License, which permits use, sharing, adaptation, distribution and reproduction in any medium or format, as long as you give appropriate credit to the original author(s) and the source, provide a link to the Creative Commons licence, and indicate if changes were made. The images or other third party material in this article are included in the article's Creative Commons licence, unless indicated otherwise in a credit line to the material. If material is not included in the article's Creative Commons licence and your intended use is not permitted by statutory regulation or exceeds the permitted use, you will need to obtain permission directly from the copyright holder. To view a copy of this licence, visit http://creativecommons.org/licenses/by/4.0/.

References

1. Kim, K., Yeom, T.: Numerical study on channel-flow convection heat transfer enhancement with piezoelectric fans under various operating conditions. Appl. Therm. Eng. **219**, 119674 (2023). https://doi.org/10.1016/j.applthermaleng.2022.119674
2. Cheng, H.-C., Chen, W.-H., Cheng, H.-F.: Theoretical and experimental characterization of heat dissipation in a board-level microelectronic component. Appl. Therm. Eng. **28**, 575–588 (2008). https://doi.org/10.1016/j.applthermaleng.2007.04.013
3. Sharma, U., Gupta, N., Saxena, K.K.: Comparative study on the effect of industrial by-products as a replacement of cement in concrete. Mater. Today: Proc. **44**, 45–51 (2021). https://doi.org/10.1016/j.matpr.2020.06.211
4. Muvvala, P., Bandhu, D.: The influence of flow blockage elements at the orifice exit on the hydrodynamic and thermal performances of impinging square jets - an experimental investigation. Heat Mass Transf. (2023). https://doi.org/10.1007/s00231-023-03371-x
5. Rajput, S.K., Kumar, J., Mehta, Y., Soota, T., Saxena, K.K.: Microstructural evolution and mechanical properties of 316L stainless steel using multiaxial forging. Adv. Mater. Process. Technol. **6**, 509–518 (2020). https://doi.org/10.1080/2374068x.2020.1728641
6. Jha, P., Shaikshavali, G., Mg, S., Mds, R., Bandhu, D., Saxena, K.K., Buddhi, D., Mk, A.: A hybrid ensemble learning model for evaluating the surface roughness of AZ91 alloy during the end milling operation. Surf. Rev. Lett. (2023). https://doi.org/10.1142/S0218625x23400012
7. Liu, Z.H., Yang, X.F., Guo, G.L.: Influence of carbon nanotube suspension on the thermal performance of a miniature thermosyphon. Int. J. Heat Mass Transf. **53**(9–10), 1914–1920 (2010). https://doi.org/10.1016/j.ijheatmasstransfer.2009.12.065
8. SanthiSree, N., Sudheer, N.V.V.S., Bhramara, P.: Analysis of closed loop pulsating heat pipe using optimization techniques. Int. J. Ambient Energy (2020). https://doi.org/10.1080/01430750.2020.1778525
9. Gunnasegaran, P., Abdullah, M.Z., Yusoff, M.Z., Abdullah, S.F.: Optimization of SiO_2 nanoparticle mass concentration and heat input on a loop heat pipe. Case Stud. Thermal Eng. **6**, 238–250 (2015). https://doi.org/10.1016/j.csite.2015.10.004
10. Tharayil, T., Asirvatham, L.G., Ravindran, V., Wongwises, S.: Thermal performance of miniature loop heat pipe with graphene–water nanofluid. Int. J. Heat Mass Transf. **93**, 957–968 (2016). https://doi.org/10.1016/j.ijheatmasstransfer.2015.11.011
11. Senthilraja, S., Vijayakumar, K., Gangadevi, R.: A comparative study on thermal conductivity of Al_2O_3/water, CuO/water and Al_2O_3–CuO/water nanofluids. Dig. J. Nanomater. Biostruct. **10**(4), 1449–1458 (2015)
12. Ramachandran, R., Ganesan, K., Rajkumar, M.R., Asirvatham, L.G., Wongwises, S.: Comparative study of the effect of hybrid nanoparticle on the thermal performance of cylindrical screen mesh heat pipe. Int. Commun. Heat Mass Transf. **76**, 294–300 (2016). https://doi.org/10.1016/j.icheatmasstransfer.2016.05.030.21
13. Jafari, D., Shamsi, H., Filippeschi, S., Di Marco, P., Franco, A.: An experimental investigation and optimization of screen mesh heat pipes for low-mid temperature applications. Exp. Thermal Fluid Sci. **84**, 120–133 (2017). https://doi.org/10.1016/j.expthermflusci.2017.02.005
14. Gupta, N.K., Barua, A., Mishra, S., Singh, S.K., Tiwari, A.K., Ghosh, S.K.: Numerical study of CeO_2/H_2O nanofluid application on thermal performance of heat pipe. Mater. Today: Proc. **18**, 1006–1016 (2019). https://doi.org/10.1016/j.matpr.2019.06.541
15. Naresh, Y.: Numerical investigation on the heat transfer performance and optimization of a finned heat pipe using artificial neural networks and genetic algorithm. Int. J. Ambient Energy (2020). https://doi.org/10.1080/01430750.2020.1727950
16. Liu, Z., Zhu, Q.: Application of aqueous nanofluids in a horizontal mesh heat pipe. Energy Convers. Manage. **52**(1), 292–300 (2011). https://doi.org/10.1016/j.enconman.2010.07.001
17. Liu, Z.H., Li, Y.Y.: A new frontier of nanofluid research–application of nanofluids in heat pipes. Int. J. Heat Mass Transf. **55**(23–24), 6786–6797 (2012). https://doi.org/10.1016/j.ijheatmasstransfer.2012.06.086
18. Kole, M., Dey, T.K.: Thermophysical and pool boiling characteristics of ZnO-ethylene glycol nanofluids. Int. J. Therm. Sci. **62**, 61–70 (2012). https://doi.org/10.1016/j.ijthermalsci.2012.02.002
19. Asirvatham, L.G., Nimmagadda, R., Wongwises, S.: Heat transfer performance of screen mesh wick heat pipes using silver–water nanofluid. Int. J. Heat Mass Transf. **60**, 201–209 (2013). https://doi.org/10.1016/j.ijheatmasstransfer.2012.11.037
20. Putra, N., Saleh, R., Septiadi, W.N., Okta, A., Hamid, Z.: Thermal performance of biomaterial wick loop heat pipes with water-based Al_2O_3 nanofluids. Int. J. Therm. Sci. **76**, 128–136 (2014). https://doi.org/10.1016/j.ijthermalsci.2013.08.020
21. Kumaresan, G., Venkatachalapathy, S., Asirvatham, L.G., Wongwises, S.: Comparative study on heat transfer characteristics of sintered and mesh wick heat pipes using CuO nanofluids. Int. Commun. Heat Mass Transfer **57**, 208–215 (2014). https://doi.org/10.1016/j.icheatmasstransfer.2014.08.001
22. Wan, Z., Deng, J., Li, B., Xu, Y., Wang, X., Tang, Y.: Thermal performance of a miniature loop heat pipe using water–copper nanofluid. Appl. Therm. Eng. **78**, 712–719 (2015). https://doi.org/10.1016/j.applthermaleng.2014.11.010
23. Kim, H.J., Lee, S.H., Kim, S.B., Jang, S.P.: The effect of nanoparticle shape on the thermal resistance of a flat-plate heat pipe using acetone-based Al_2O_3 nanofluids. Int. J. Heat Mass Transf. **92**, 572–577 (2016). https://doi.org/10.1016/j.ijheatmasstransfer.2015.09.013
24. Mahdavi, M., Tiari, S., De Schampheleire, S., Qiu, S.: Experimental study of the thermal characteristics of a heat pipe. Exp. Therm. Fluid Sci. **93**, 292–304 (2018). https://doi.org/10.1016/j.expthermflusci.2018.01.003
25. Solomon, A.B., Ramachandran, K., Pillai, B.C.: Thermal performance of a heat pipe with nanoparticles coated wick. Appl. Therm. Eng. **36**, 106–112 (2012). https://doi.org/10.1016/j.applthermaleng.2011.12.004
26. Moraveji, M.K., Razvarz, S.: Experimental investigation of aluminum oxide nanofluid on heat pipe thermal performance. Int.

Commun. Heat Mass Transf. **39**(9), 1444–1448 (2012). https://doi.org/10.1016/j.icheatmasstransfer.2012.07.024
27. Reddy, P.L., Reddy, B.S., Govindarajulu, K.: Thermal performance prediction of heat pipe with TiO_2 nanofluids using RSM. Therm. Sci. **26**(1), 641–651 (2022). https://doi.org/10.2298/TSCI201229199R
28. Sarafraz, M.M., Pourmehran, O., Yang, B., Arjomandi, M.: Assessment of the thermal performance of a thermosyphon heat pipe using zirconia-acetone nanofluids. Renew. Energy **136**, 884–895 (2019). https://doi.org/10.1016/j.renene.2019.01.035
29. Khajehpour, E., Noghrehabadi, A.R., Nasab, A.E., Nabavi, S.H.: Experimental investigation of the effect of nanofluids on the thermal resistance of a thermosiphon L-shape heat pipe at different angles. Int. Commun. Heat Mass Transf. **113**, 104549 (2020). https://doi.org/10.1016/j.icheatmasstransfer.2020.104549
30. Khoobbakht, G., Najafi, G., Karimi, M., Akram, A.: Optimization of operating factors and blended levels of diesel, biodiesel and ethanol fuels to minimize exhaust emissions of diesel engine using response surface methodology. Appl. Therm. Eng. **99**, 1006–1017 (2016). https://doi.org/10.1016/j.applthermaleng.2015.12.143
31. Reddy, P.L., Reddy, B.S., Govindarajulu, K.: Research on water based nano fluids effecting thermal performance of heat pipe. Int. J. Recent Technol. Eng. **2**(8), 5245–5250 (2019)
32. Gunnasegaran, P., Abdullah, M.Z., Shuaib, N.H.: Influence of nanofluid on heat transfer in a loop heat pipe. Int. Commun. Heat Mass Transf. **47**, 82–91 (2013). https://doi.org/10.1016/j.icheatmasstransfer.2013.07.003
33. Vidhya, R., Balakrishnan, T., Kumar, B.S.: Experimental and theoretical investigation of heat transfer characteristics of cylindrical heat pipe using Al_2O_3–SiO_2/W-EG hybrid nanofluids by RSM modeling approach. J. Eng. Appl. Sci. **68**(1), 1–20 (2021)
34. Beiginaloo, G., Mohebbi, A., Afsahi, M.M.: Combination of CFD and DOE for optimization of thermosyphon heat pipe. Heat. Mass Transf. **58**, 1–14 (2022)
35. Adin, M.Ş, Okumuş, M.: Investigation of microstructural and mechanical properties of dissimilar metal weld between AISI 420 and AISI 1018 STEELS. Arab. J. Sci. Eng. **47**(7), 8341–8350 (2022)
36. Adin, M.Ş: A parametric study on the mechanical properties of MIG and TIG welded dissimilar steel joints. J. Adhes. Sci. Technol. (2023). https://doi.org/10.1080/01694243.2023.2221391
37. Adin, M.Ş: Performances of cryo-treated and untreated cutting tools in machining of AA7075 aerospace aluminium alloy. Eur. Mech. Sci. **7**(2), 70–81 (2023)
38. Altun, Ş, Adin, M.Ş, İlçin, K.: Monohydric aliphatic alcohols as liquid fuels for using in internal combustion engines—a review. Proc. Inst. Mech. Eng., Part E: J. Process Mech. Eng. (2023). https://doi.org/10.1177/09544089231160472
39. Adin, M.Ş, Altun, Ş, Adin, M.Ş: Effect of using bioethanol as fuel on start-up and warm-up exhaust emissions from a diesel power generator. Int. J. Ambient Energy **43**(1), 5711–5717 (2022)
40. Ghanbarpour, M., Nikkam, N., Khodabandeh, R., Toprak, M.S.: Thermal performance of inclined screen mesh heat pipes using silver nanofluids. Int. Commun. Heat Mass Transf. **67**, 14–20 (2015). https://doi.org/10.1016/j.icheatmasstransfer.2015.06.009
41. Reddy, P.L., Reddy, B.S. and Govindarajulu, K.: Parametric optimization for better thermal performance on Heat Pipe using Taguchi method. In: IOP Conference Series: Materials Science and Engineering (Vol. 993, No. 1, p. 012145). IOP Publishing. (2020). doi:https://doi.org/10.1088/1757-899X/993/1/012145
42. Babaki, M., Yousefi, M., Habibi, Z., Mohammadi, M.: Process optimization for biodiesel production from waste cooking oil using multi-enzyme systems through response surface methodology. Renew. Energy **105**, 465–472 (2017)
43. Bandhu, D., Kumari, S., Prajapati, V., Saxena, K.K., Abhishek, K.: Experimental investigation and optimization of RMD™ welding parameters for ASTM A387 grade 11 steel. Mater. Manuf. Process. **36**, 1524–1534 (2020). https://doi.org/10.1080/10426914.2020.1854472
44. Agarwal, K.M., Tyagi, R.K., Saxena, K.K.: Deformation analysis of Al Alloy AA2024 through equal channel angular pressing for aircraft structures. Adv. Mater. Process. Technol. **8**, 828–842 (2020). https://doi.org/10.1080/2374068x.2020.1834756
45. Awasthi, A., Saxena, K.K., Arun, V.: Sustainable and smart metal forming manufacturing process. Mater. Today: Proc. **44**, 2069–2079 (2021). https://doi.org/10.1016/j.matpr.2020.12.177

Publisher's Note Springer Nature remains neutral with regard to jurisdictional claims in published maps and institutional affiliations.